Electronic Supplementary Material

Supported High and Medium Entropy Nano Alloys from MOFs Catalyze Alkene Oxidation Reaction

Alejandro Lumbreras–Teijeiro,[a] Anna Nowacka,[a] Alejandro Serrano–Maldonado,[a] Matthijs A. van Spronsen,[b] Judit Oliver–Meseguer,[a,*] Antonio Leyva–Pérez.[a,*]

[a] Instituto de Tecnología Química. Universitat Politècnica de València–Agencia Estatal Consejo Superior de Investigaciones Científicas. Avda. de los Naranjos s/n, 46022, València, Spain.

[b] Diamond Light Source Ltd., Harwell Science and Innovation Campus, Chilton, Didcot, OX11 0DE, United Kingdom

Corresponding authors: joliverm@itq.upv.es, anleyva@itq.upv.es

Table of Contents

1. Supplemental experimental procedures

1.1 General experimental methods.

Reagents were obtained from commercial sources (Merck-Aldrich) and used without further purification otherwise indicated. Glassware was dried in an oven at 100°C before use. Reactions were typically performed in 6.0 mL reactors equipped with a magnetic stirrer and closed with a plastic cap having a rubber septum part to sample out, and placed in steel heaters. All the products obtained were characterized by GC connected to a FID detector, GC-MS and IR, ^{1}H, ^{13}C NMR and DEPT when needed. When available, the characterization given in the literature was used for comparison. Gas chromatographic analyses were performed in an instrument equipped with a 25 m capillary column of 5% phenylmethyl silicone. *N*-dodecane was used as an internal standard. GC-MS analyses were performed on a spectrometer equipped with the same column as the GC and operated under the same conditions. Preparative chromatography and TLC were performed over SiO_2. ^{1}H, ^{13}C NMR, and DEPT were recorded in a 400 MHz instrument using $CDCl_3$ as a solvent, containing TMS as an internal standard. IR spectra of the compounds were recorded on a spectrophotometer by impregnating the windows with an ether solution of the compound and letting to evaporate before analysis.

XDR measurements are carried out with PANalytical Cubix-Pro diffractometer, equipped with PANalytical X'Celerator detector, with monochromatic CuK_α (λ_1 = 1.5406 Å, λ_2 = 1.5444 Å, I_2/I = 0.5), voltage and tube intensity of 45 kV and 40 mA respectively.

Transmission Electron Microscopy analysis are performed with a JEOL JEM 2100F of 200 kV. The instrument is equipped with STEM unity and BF and DF (HAADF) detectors. Chemical characterization is performed with a EDS X-Max 80 detector from Oxford Instruments, with 127 eV resolution.

Metal content analysis are performed in an Inductively Coupled Plasma instrument (ICP-AES) from Thermo Scientific, model iCAP-PRO.

The surface area was determined by the Brunauer-Emmet-Teller (BET) method and the micropore volume was determined by the t-plot method applied to nitrogen adsorption isotherms measured at − 196 °C on the volumetric device

Micromeritics ASAP 2420 after degassing the samples at 400 °C under vacuum for 12 h.

Near-ambient pressure (NAP) X-ray photoelecton spectroscopy (XPS) and X-ray absorption spectroscopy (XAS) measurements. A suspension was made of the high and medium-entropy alloy (HMEA) powder (post 800°C anneal, HMEA-800) in ethanol. This suspension was drop cast onto a piece of Au foil (99.99% purity, 0.5-mm thickness, temper as rolled, Advent Research Materials). Prior to drop casting, the Au foil was cleaned three times with isopropanol and purged with N_2(g).

The prepared sample was introduced in the high-vacuum “TCUP” endstation of beamline B07C, the Diamond Light Source, United Kingdom. Briefly, this bending-magnet beamline is designed for near-ambient pressure (NAP) X-ray photoelecton spectroscopy (XPS) and X-ray absorption spectroscopy (XAS). The X-ray radiation is collected via a plane grating monochromator (400 lines/mm and C_{ff} of 2.0) and focused on the exit slits, which were set to 0.025 mm in the energy dispersive direction (vertical) and 0.5 mm in the horizontal direction.

The sample was heated with a button heater (Heatwave Labs #101491-02), which incorporates a thermocouple. A second thermocouple was clipped atop the heater adjacent to the sample. Both, K-type, thermocouples were measured during the experiment with the one closer to the sample believe to give a more realistic representation of the sample temperature. High-purity H_2 was admitted in the endstation via Alicat mass-flow controllers from a dedicated gas-handing system, which included a butterfly valve acting as back-pressure controller set to 1 mbar (measured with a capacitance gauge). The sample was measured heated in steps to ca. 600°C in hydrogen. Spectra were collected in between heating steps close to room temperature (30–40°C) and evacuated to high vacuum.

The near-edge X-ray absorption fine structure (NEXAFS) spectra were collected by measuring the drain current from the cone of the NAP XPS hemispherical analyser, electrically isolated from ground and connected to a preamplifier (Stanford Research Systems SRS570). With the sample grounded, the cone was biased to +5.0 V to increase the signal intensity. The initial spectra were also collected via Auger electron yield using the NAP XPS Specs Phoibos 150

analyser. However, no differences were found between Auger and total electron yield (data not shown).

To normalise the spectra to the photon flux, drain current was collected from a Au mesh upstream of the sample using another SRS570 preamplifier. For the C K edge spectra, C species on the Au mesh precluded this, and instead, the beamline transmission curve was used. The latter is measured periodically on the beamline by backfilling the chamber with He (2 mbar) and recording the photoemission current while changing the photon energy. This was then normalised to the He photoionisation cross section and the ring current. The C K edge spectra were divided by the transmission curve and the beam current. For calibration of the photon-energy axis, several references were used. For the C K edge spectra, the strong π^* resonance on the Au mesh, measured simultaneously with every C K edge scan, provided a good energy reference. This species was determined to be 285.23 eV (referenced to the 1s-3p resonance of CH_4(g), earlier reported to be at 288.0 eV.

1.2 Reaction procedures

Synthesis of MOF **1**

Synthesis of MOF **1** were performed according to previously reported procedure Briefly, 1 mmol of each metal salts: $Co(NO_3)_2{\cdot}6H_2O$, $Ni(NO_3)_2{\cdot}6H_2O$, $Zn(NO_3)_2{\cdot}6H_2O$, $Mn(NO_3)_2{\cdot}4H_2O$, $Fe(SO_4)$ or $FeCl_2$, and 2,5 mmol of organic linker H_4DOT were dissolved in 60 mL DMF/EtOH/water (in a 15:1:1 ratio respectively) and heated to 120 °C for 20–24 h in an autoclave. The resulting crystals were washed 3 times with 50 mL of fresh DMF solvent, and soaked in MeOH for solvent exchange (3 exchanges over a 3 day period). Resulted material were then activated to remove all solvent by evacuating under vacuum (100-200 mTorr) overnight at 80°C.

Synthesis of HMEA-NPs

A portion of MOF **1** was transferred to the quartz tube reactor and connected to vertical calcination oven equipped with the N_2. Gas flow was set up 100 mL/min for each experiment. The temperature and heating ramp was adjusted separately for each experiment. The same sample of material was pyrolyzed at different temperatures 400 ºC (5 ºC/min), 550 ºC (5 ºC/min), 700 ºC (5 ºC/min) and 800 ºC

(10 ºC/min) for 5h. Pyrolysis at all temperatures (except 800 ºC) were followed by reduction in H_2 (100 mL/min) at 400 ºC for 4h. After each pyrolysis, small portion of material was separated and saved for further characterization, in order to follow morphological changes in the examined material.

Synthesis of Metal-C-NPs

A round bottom flask containing the one of the selected nitrate salts: $Mn(NO_3)_2{\cdot}4H_2O$, $Co(NO_3)_2{\cdot}6H_2O$, $Ni(NO_3)_2{\cdot}6H_2O$, $Fe(NO_3)_3{\cdot}9H_2O$ or $Zn(NO_3)_2{\cdot}6H_2O$ (1.8 mmol) and methanol (50 mL) is placed in an ultrasonic bath for 5 minutes. Active carbon (1g) is added, and the suspension is sonicated for 2 h at rt. Then, methanol was removed on a rotary evaporator, adjusting the bath temperature at 40 °C. The solid was transferred to a crystallizing dish and dried at 100 °C for 12 h. Then, the reaction mixture was cooled down to room temperature and grounded to a powder. The powder was placed in a quartz glass tube reactor and connected to vertical reduction oven. The reactor was flushed with N_2 for 10 min and then reduced with H_2 (100 mL/min) at 400 °C for 4 h (heating ramp 5 °C/min). As-prepared carbon-supported catalytic materials were characterized by ICP-OES and powder X-ray diffraction.

General procedure for the oxidative cleavage of styrene derivatives catalysed by HMEA-700 NPs.

Typically, styrene or styrene derivative (1 mmol), hexane (1 mL, 1M) and HMEA-700 (2.5 mg) are placed in a reactor flask containing a stirring bar. Then, *tert*-butyl hydroperoxide solution 5.0 – 6.0 M in *n*-dodecane (3-5 mmol) is added and the reaction is stirred at 67 ºC or the desired temperature for 18-20 h. distilled water is added for quenching the reaction, extracted with diethyl ether and filtrated if necessary. The products are analysed by GC, GC-MS and NMR in order to determine its structure.

1.3 Compound characterization

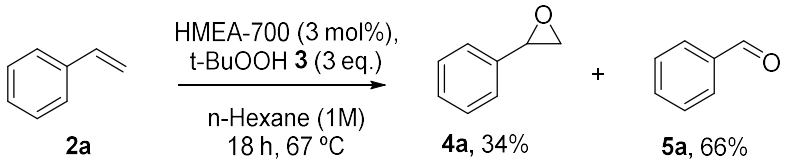

1-Methyl-4-vinylbenzene (**2a**) oxidative cleavage: Following the typical reaction procedure described, 1 mmol (104 mg) of starting material **1a** did undergo catalytic oxidative cleavage within 100 % conversion, obtaining product **5a** (benzaldehyde) in 34 % yield, **4a** (2-phenyloxirane) in 66 % yield.

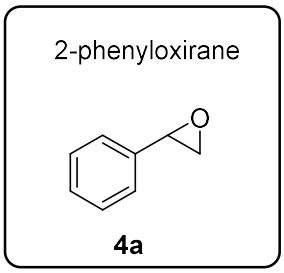

GC-MS (m/z, relative intensity): 120 ($M^{+\bullet}$, 37), 119 (55), 91 (100), 90 (68), 89 (81), 63 (28), 51 (19), 39 (15).

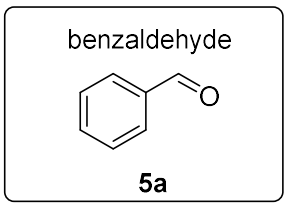

GC-MS (m/z, relative intensity): 106 ($M^{+\bullet}$, 100), 105 (98), 77 (90), 51 (48).

1-Methyl-4-vinylbenzene (**2b**) oxidative cleavage: Following the typical reaction procedure described, 1 mmol (118 mg) of starting material **2b** did undergo catalytic oxidative cleavage within 99 % conversion, obtaining product **5b** in 44 yield % and product **4b** in 55%.

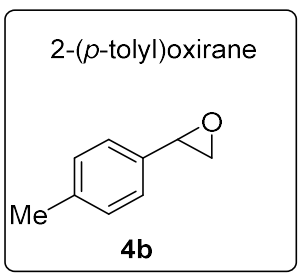

GC-MS (m/z, relative intensity): 134 ($M^{+\bullet}$, 21), 105 (100), 91 (15), 79 (15), 77 (22), 63 (9), 51 (9).

4-methylbenzaldehyde

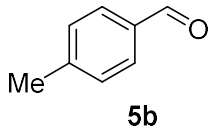

5b

GC-MS (m/z, relative intensity): 120 ($M^{+\bullet}$, 74), 119 (100), 91 (87), 65 (35), 63 (17), 62 (13), 39 (10).

(*E*)-Prop-1-en-1-ylbenzene (**2c**) oxidative cleavage: Following the typical reaction procedure described, 1 mmol (118 mg) of starting material **2c** did undergo catalytic oxidative cleavage within 93 % conversion, obtaining product **4c** in 93 % yield.

2-methyl-3-phenyloxirane

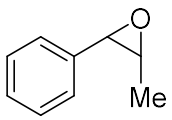

4c

GC-MS (m/z, relative intensity): 134 ($M^{+\bullet}$, 34), 133 (51), 90 (100), 89 (94).

4-Vinylbenzoic acid (**2d**) oxidative cleavage: Following the typical reaction procedure described,1 mmol (148 mg) of starting material **2d** did undergo catalytic oxidative cleavage within 82 % conversion, obtaining product **5d** in 82 % yield.

4-formylbenzoic acid

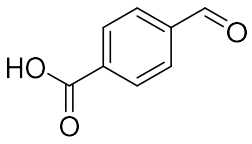

5d

GC-MS (m/z, relative intensity): 164 ($M^{+\bullet}$, 69), 163 (36), 133 (100), 105 (19), 77 (34), 51 (25), 28 (9).

1-Methyl-3-vinylbenzene (**2e**) oxidative cleavage: Following the typical reaction procedure described,1 mmol (118 mg) of starting material **1e** did undergo catalytic oxidative cleavage within 88 % conversion, obtaining product **4e** in 21 % yield and product **5e** in 51 % yield.

2-(m-tolyl)oxirane

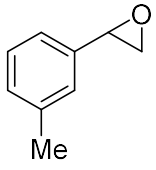

4e

GC-MS (m/z, relative intensity): 134 ($M^{+\bullet}$, 24), 119 (10), 106(23), 105 (100), 103 (23), 91 (25), 77 (25), 63 (14), 51 (15), 39 (12), 28 (9).

3-methylbenzaldehyde

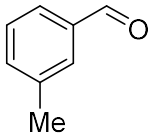

5e

GC-MS (m/z, relative intensity): 120 ($M^{+\bullet}$, 97), 119 (72), 91 (100), 65 (32), 50 (17), 39 (18), 28 (19).

1-Bromo-4-vinylbenzene (**2f**) oxidative cleavage: Following the typical reaction procedure described,1 mmol (183 mg) of starting material **2f** did undergo catalytic oxidative cleavage within 92 % conversion, obtaining product **5f** in 92 % yield.

4-bromobenzaldehyde

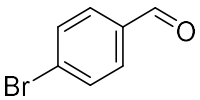

5f

GC-MS (m/z, relative intensity): 186 ($M^{+\bullet}$, 65), 185 (100), 184 (100), 183 (96), 157 (28), 155 (59), 104 (10), 77 (54), 76 (49), 75 (42), 74 (49), 51 (26), 50 (49), 28 (15).

4-Allyl-1,2-dimethoxybenzene (**2g**) oxidative cleavage: Following the typical reaction procedure described,1 mmol (178 mg) of starting material **2g** did undergo catalytic oxidative cleavage within 80 % conversion, obtaining product **5g-1** in 27 % yield **5g-2** in 33 % yield.

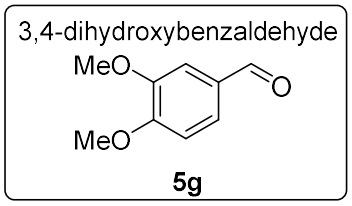

GC-MS (m/z, relative intensity): 166 ($M^{+\bullet}$, 100), 165 (100), 151 (14), 121 (19), 95 (41), 77 (22), 74 (20), 65 (14), 51 (20), 39 (9), 28 (10).

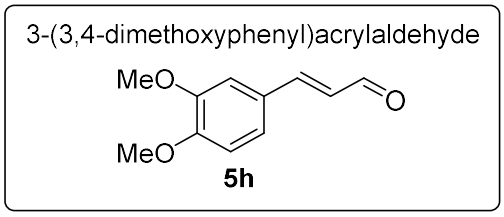

GC-MS (m/z, relative intensity): 192 ($M^{+\bullet}$, 100), 177 (21), 167 (25), 161 (100), 151 (33), 149 (45), 138 (17), 121 (31), 106 (20), 103 (20), 91 (47), 78 (39), 77 (51), 63 (22), 51 (30), 43 (16), 28 (26).

2. Supplemental Tables and Figures

Table S1 Inductively coupled plasma optical emission spectroscopy (ICP-OES) results of the different mixed-metal MOF **1** batches.

	Batch 1 (mol%)	**Batch 2 (mol%)**	**Batch 3 (mol%)**
Ni	27.4	22.4	24.8
Co	27.4	23.8	27.0
Fe	19.2	30.5	24.5
Mn	15.9	7.6	23.8
Zn	10.1	15.7	6.0

Table S2 Catalytic results throughout the reuses for the oxidation of styrene **2a** with *t*–BuOOH **3** (3 equivalents) catalysed by HMEA–700 (3 mol%) in *n*–hexane as a solvent. See Figure 8 in the main text for details.

Use	Conversion of 2a (%)	4a (%)	5a (mol%)
1	97	82	15
2	95	81	14
3	94	81	13
4	95	83	12
5	87	77	10
6	93	82	11
7	79	69	10
8	77	68	9
9	81	70	11
10	78	68	10

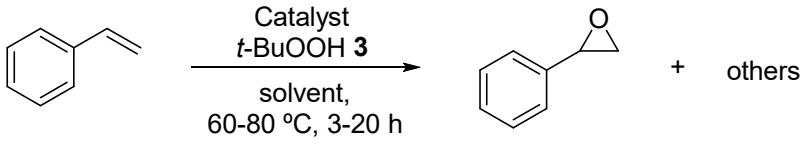

2a **4a**

Table S3 Reported catalysts and results for the oxidation of styrene **2a** to give product **4a** with *t*–BuOOH **3**, typically at 60-80 ºC for 3-20 h.

Catalytic system	Solvent	Yield (%)	Ref.
Dioxomolybdenum(VI) complex with salicylamide ligands	No solvent	86	S1
$Pd(OAc)_2$, K_2CO_3	Dichloromethane	85	S2
Ti-MCM41	Acetonitrile	79	S3
Ta-MCM41	Acetonitrile	69	S3
Nanogold on carbon	No solvent	62	S4
Molybdenum maltolate	No solvent	55	S5
Bismuth copper oxide	Acetonitrile	52	S6
I_2, Na_2CO_3	Acetonitrile	51	S7
Tungstate polyoxometalate	Chloroform, dimethylformamide	14	S8

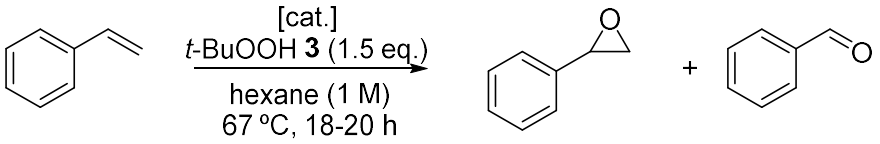

2a **4a** **5a**

Table S4 Comparative of oxidative cleavage catalysed by HMEA-700, Mn(C), Co(C) and the physical mixture of all individual metals with 3 equivalents of *t*-BuOOH. Conversion (**2a**) and yield (**4a**, **5a**) calculated by GC, using *n*–dodecane as an internal standard. Conditions: 1 mmol styrene **2a**, 1.5 equiv. of *t*–BuOOH **3**, 1 mL hexane.

Entry	Catalyst	Metal load (mol %)					Conversion	Yield (%)	
		Mn	Co	Fe	Ni	Zn		4a	5a
1	HMEA	0.65	0.8	0.8	0.8	-	77	59	18
2	Mn-C	0.65	-	-	-	-	60	52	8
3	Co-C	-	0.8	-	-	-	71	61	10
4	Mn+Co+Ni+Fe -C	0.65	0.8	0.8	0.8		77	61	16

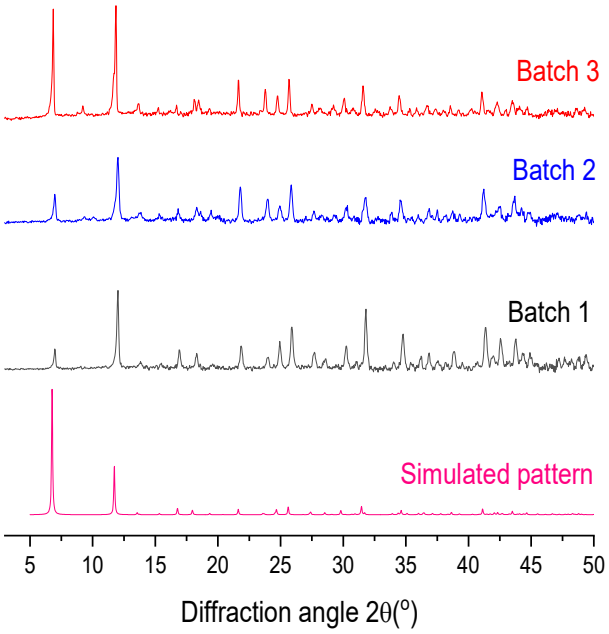

Fig. S1 Diffraction patterns of the different MOF 1 batches, compared with the simulated pattern.

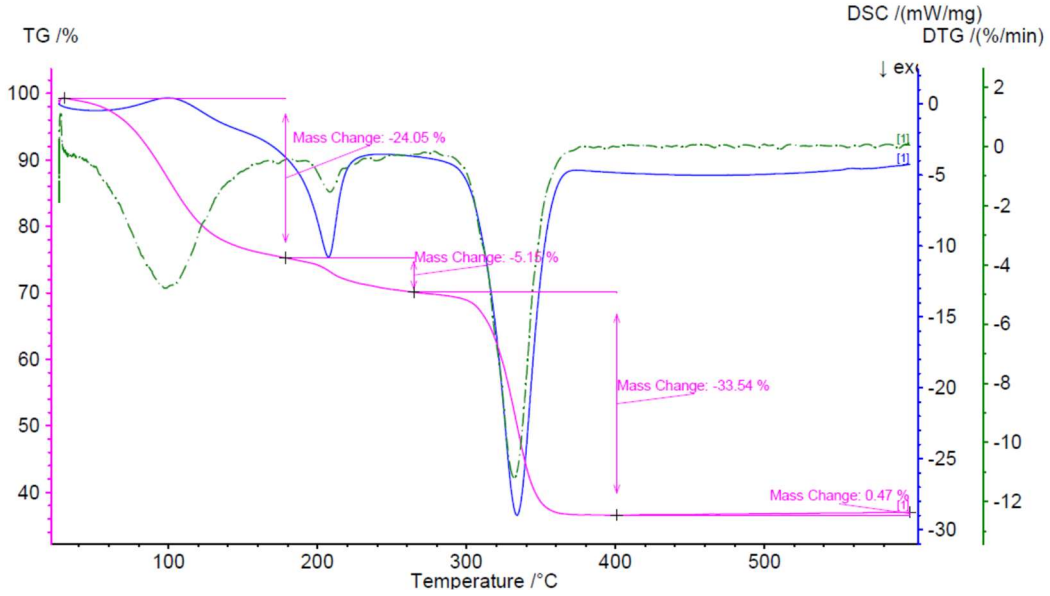

Fig. S2 Thermogravimetry differential thermal analysis (TG/DTG) and differential scanning calorimetry (DSC) of MOF **1** (batch 1).

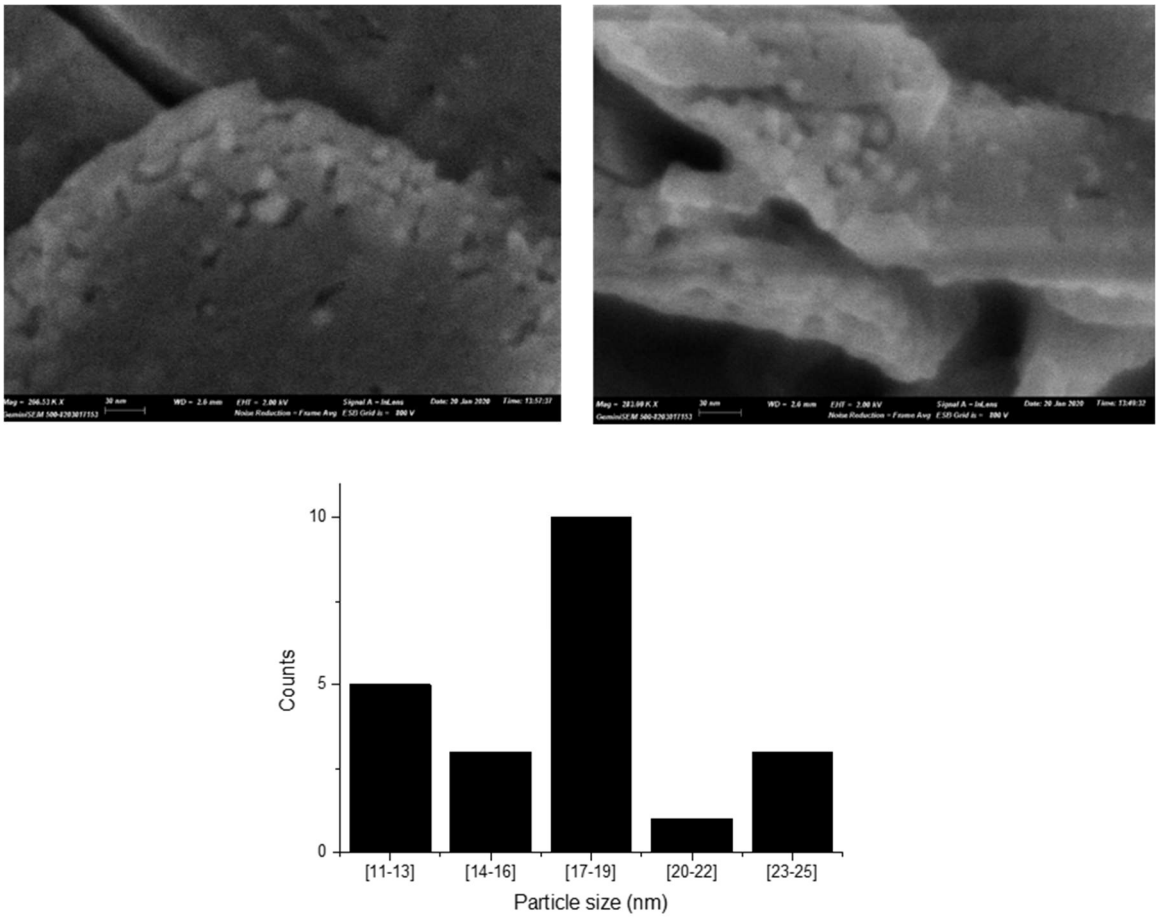

Fig. S3 High resolution-field emission scanning electron microscope (HR-FESEM) pictures of HMEA-400 (top left and right). Histogram of NPs size distribution in HMEA-400 (bottom), the y-axis shows the number of particles counted. Scale bars denote 30 nm.

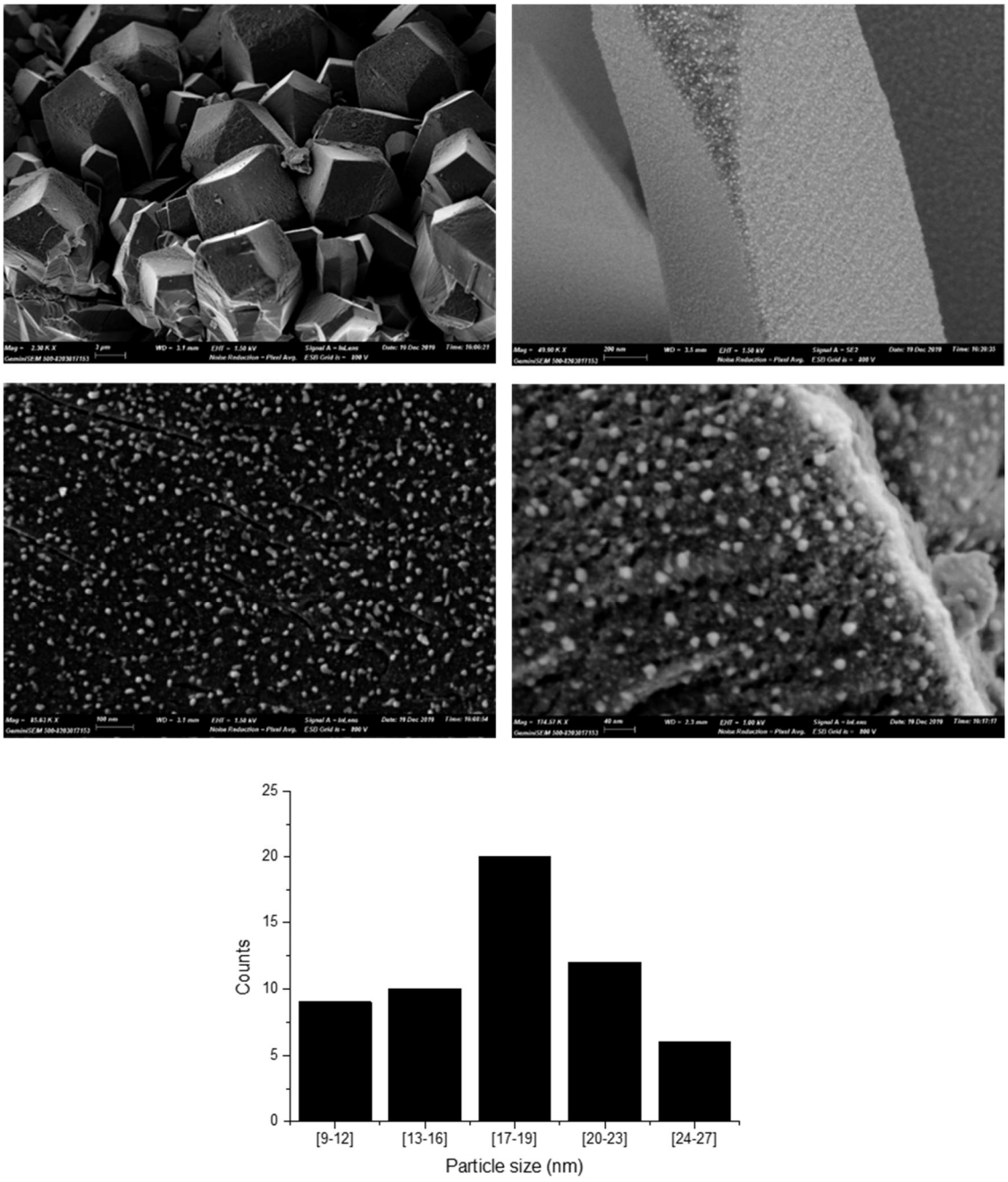

Fig. S4 High resolution-field emission scanning electron microscope (HR-FESEM) pictures of HMEA-550 (top left and right; middle left and right). Histogram of NPs size distribution in HMEA-550 (bottom), the y-axis shows the number of particles counted. Scale bars denote (from top left to bottom right): 2 μm, 200 nm, 100 nm and 40 nm.

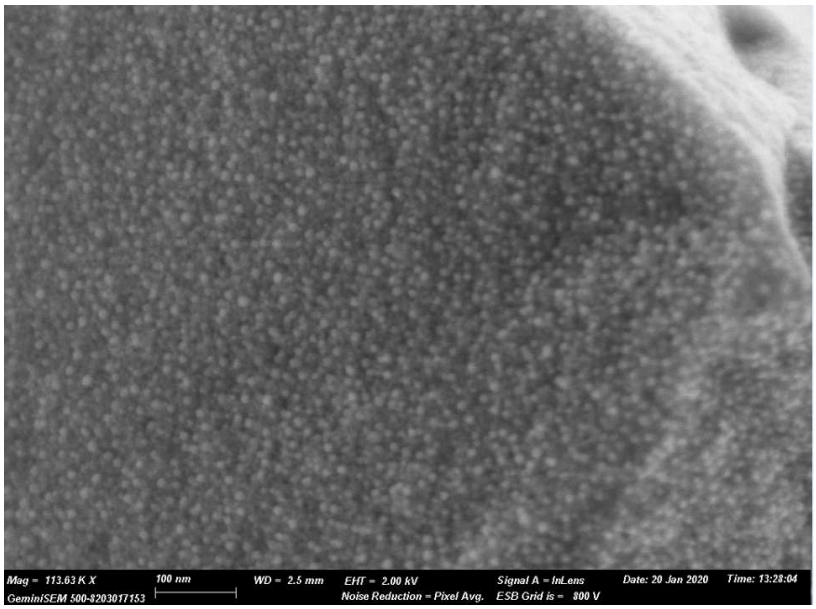

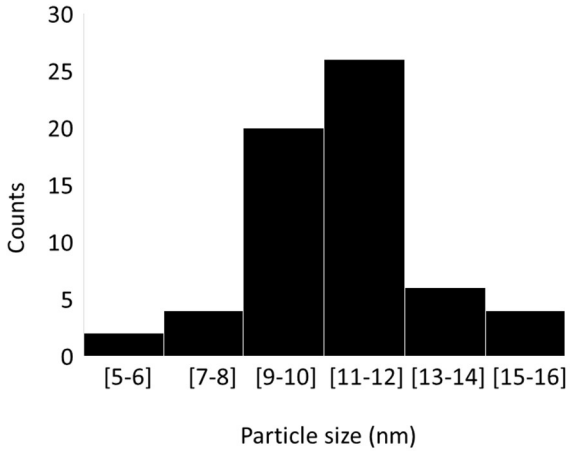

Fig. S5 High resolution-field emission scanning electron microscope (HR-FESEM) pictures of HMEA-700 (top). Histogram of NPs size distribution in HMEA-700 (bottom), the y-axis shows the number of particles counted.

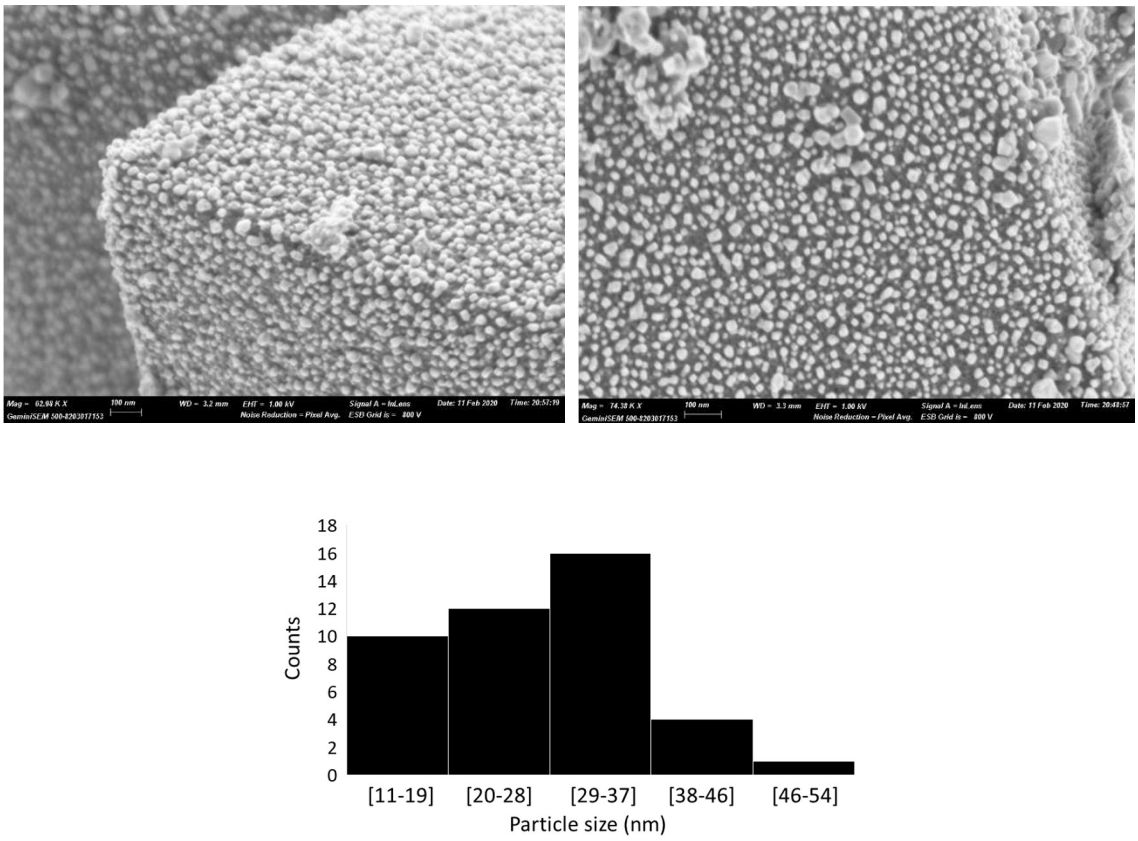

Fig. S6 High resolution-field emission scanning electron microscope (HR-FESEM) pictures of HMEA-800 (top left and right). Histogram of NPs size distribution in HMEA-800 (bottom), the y-axis shows the number of particles counted. Scale bars denote 100 nm.

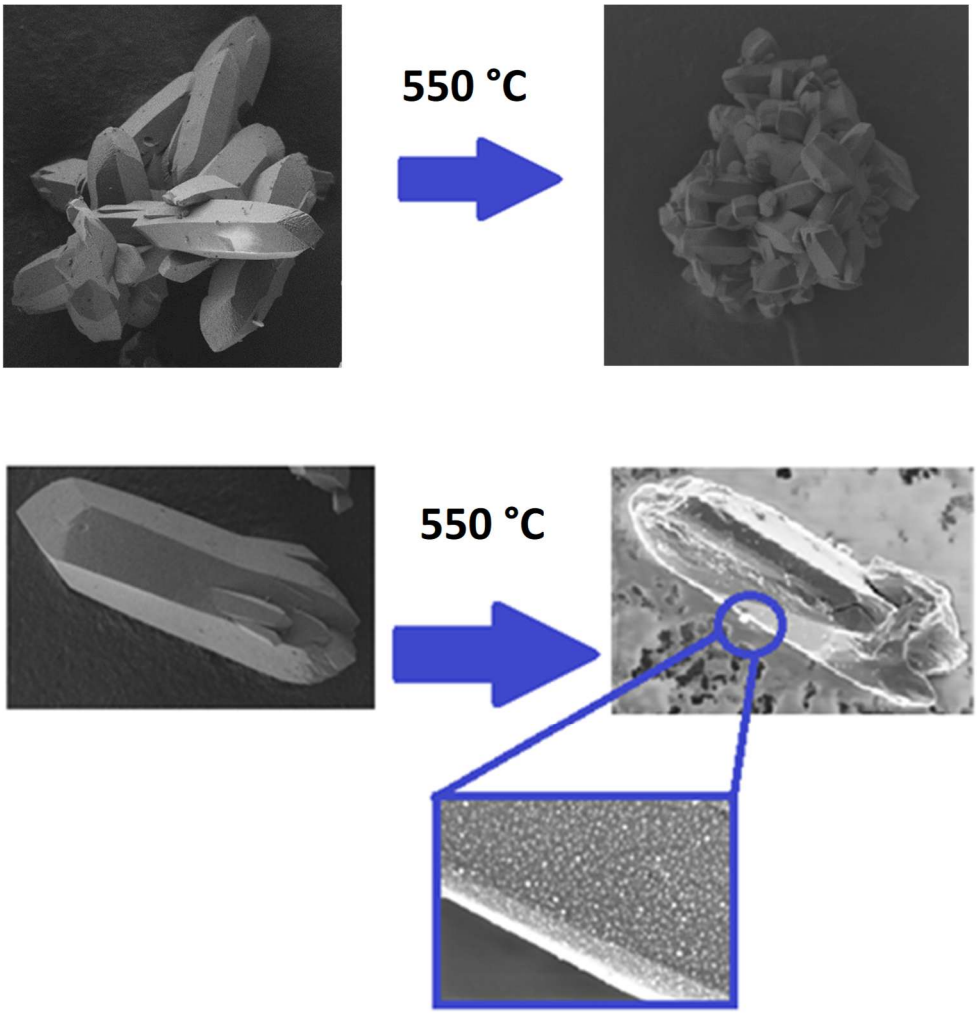

Fig. S7 Field emission scanning electron microscopic images of MOF **1** before and after the pyrolysis at 550 ºC (HMEA-550); the inset magnifies the circled area.

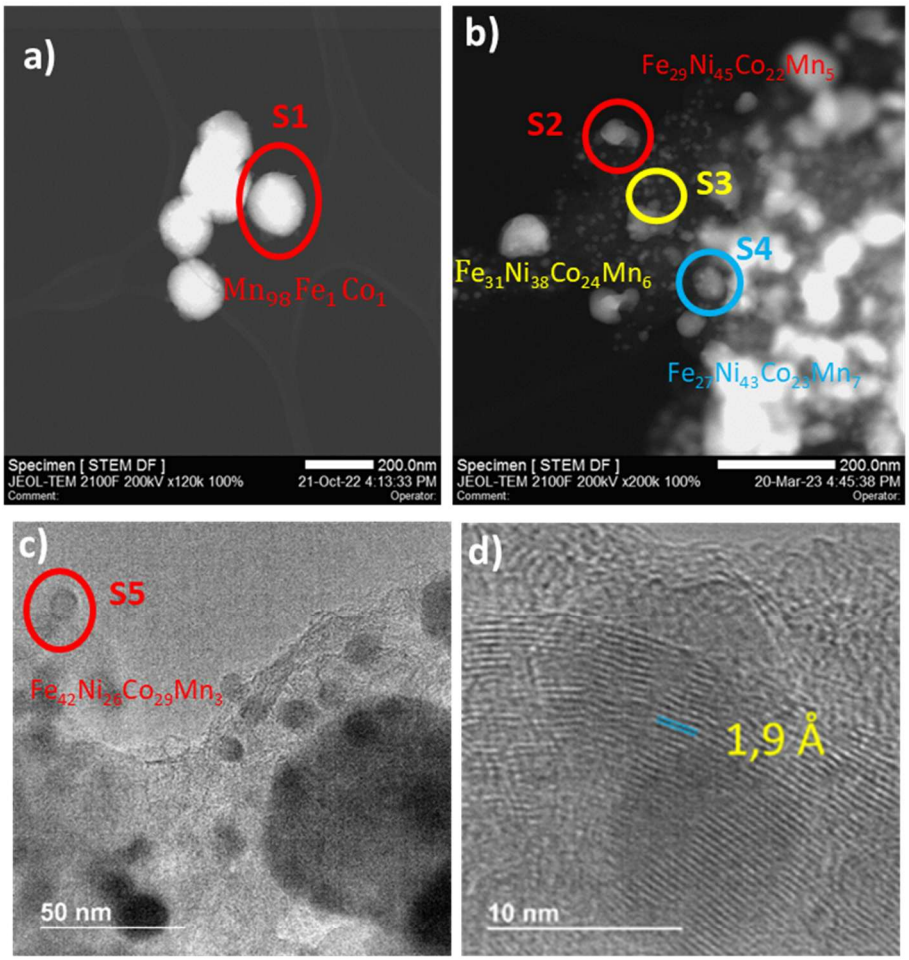

e)

EDX	Wt%				
Element	S1	S2	S3	S4	S5
Mn	98.32	4.55	6.38	7.01	3.27
Fe	1.03	29.08	31.44	26.6	41.83
Co	0.57	21.77	24.13	23.46	29.33
Ni	0.07	44.6	38.05	42.93	25.57
Zn	0	0	0	0	0

Fig. S8 (a) Dark field high-resolution scanning transmission electron microscopy (HR-STEM) picture of Mn-rich NPs of HMEA-700. (b) Dark-field HR-STEM picture of FeCoNi-rich NPs of HMEA-700. (c) HR-STEM) picture of Fe-richer NPs of HMEA-700. (d) Crystallographic plane distance found after HR-TEM image of a representative NP in the material. (e) Energy-dispersive X-ray (EDX) analysis results for selected NPs (circled and named).

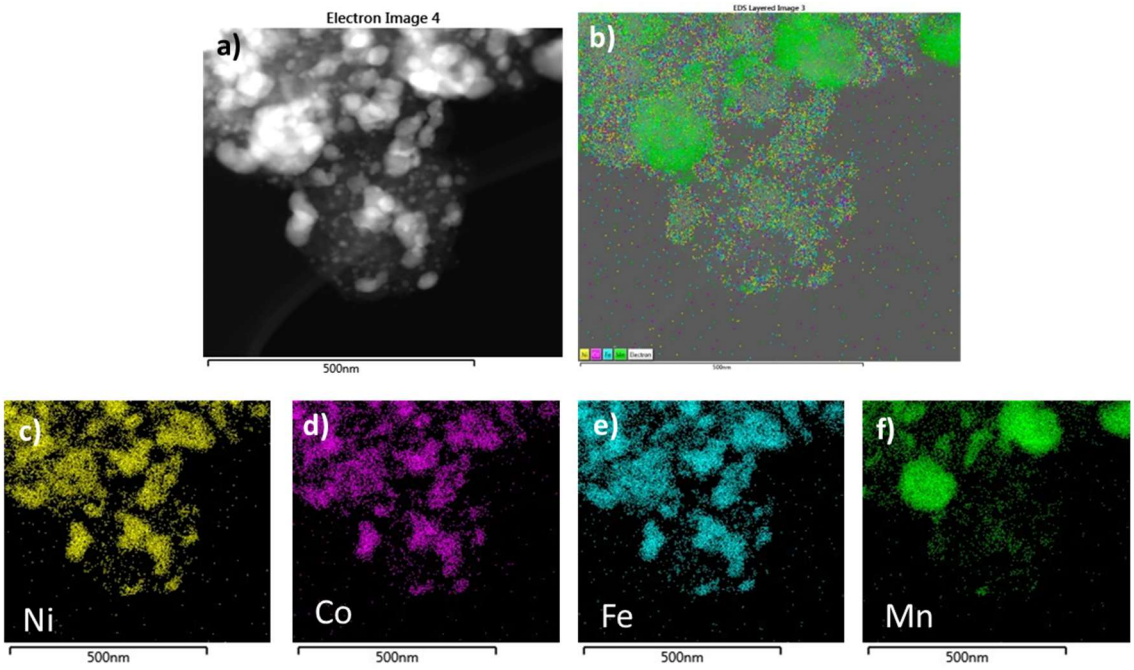

Fig. S9 (a) Dark-field scanning transmission electron microscope and energy-dispersive X-ray spectroscopy (STEM-EDX) mapping of a sample of HMEA-700. (b) Dark-field STEM image EDX-mapping overlap image of Ni, Co, Fe, and Mn of the studied region. (c-f) EDX-mapping image of Ni, Co, Fe, and Mn of the studied region.

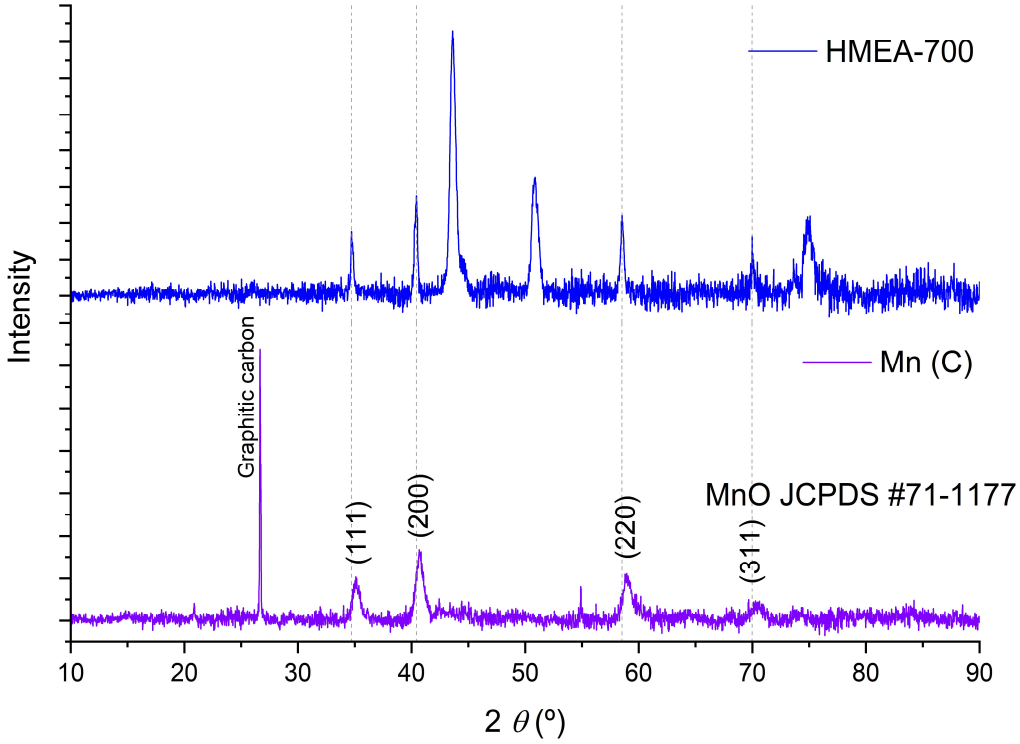

Fig. S10 Carbon–supported Mn NPs (**Mn (C)**) characterization by powder X-ray diffraction (PXRD) (bottom) and comparison with the HMEA-700 (after H_2 reduction) pattern (top). Inductively coupled plasma optical emission spectroscopy (ICP-OES) analysis indicates a concentration in Mn of 9.29 wt%.

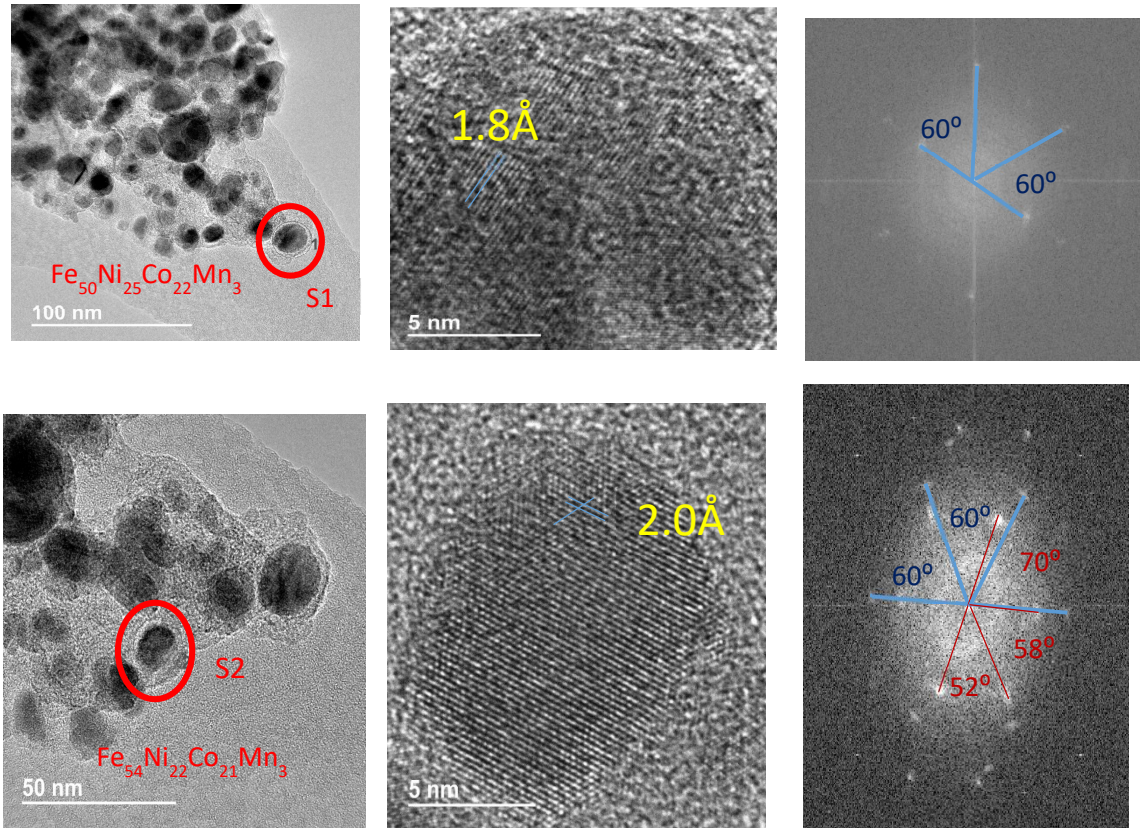

EDX	Wt%	
Element	**S1**	**S2**
Mn	2.69	3.17
Fe	50.24	54.04
Co	22.13	21.20
Ni	24.94	21.58
Zn	0.00	0.00

Fig. S11 High-resolution transmission electron microscopy (HR-TEM) pictures of HMEA-800 (top left and bottom left). Crystallographic plane distance found after HR-TEM image of a representative NP in the material (top middle and bottom middle). Fast Fourier transform (FFT) diffraction patterns (top right and bottom right) and energy-dispersive X-ray spectroscopy (EDX) analysis results of selected HMEA-800 NPs (table).

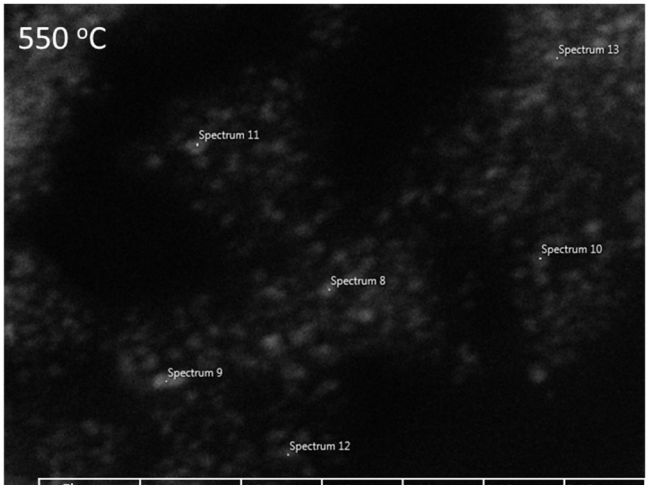

Element	S 8	S 9	S 10	S 11	S 12	S 13
Mn	22.92	4.26	0.48	15.78	36.85	67.37
Fe	28.93	43.24	8.91	23.04	22.62	10.96
Co	19.29	15.45	62.82	19.94	10.62	7.16
Ni	26.13	33.85	20.07	36.42	11.28	4.12
Zn	2.73	3.19	7.73	4.82	18.62	10.39

Fig. S12 Scanning transmission electron microscope and energy-dispersive X-ray spectroscopy (STEM-EDX) image of HMEA-550, with the corresponding EDX analysis of the indicated nanoparticles.

The entropy-based definition identifies HEAs via the mixed configuration entropy (S). The mixed configuration entropy of HEAs is able to be depicted by the following equation:

$$\Delta S = -R\sum x_i \ln(x_i) \qquad (1)$$

where R is the molar gas constant, and x_i represents the mole fraction of the elemental component. As such, S of HEAs with equal molar ratios for metallic elements in liquid state or solid solution state can be simplified:

$$\Delta S = R\ln(n) \qquad (2)$$

where n represents the number of components in the alloy. When the number of elemental components of the alloy is ≥5, the alloy with mixed configuration entropy $\Delta S \geq 1.5R$ refers to a HEA. Specifically, the maximum configurational entropy of a 5-element HEA is 1.61R (for the equimolar alloy), but the minimum value is 1.36R, and the latter may include some quaternary alloys.

Fig. S13 Definition of high- and medium-entropy alloys (HMEAs).

Co species

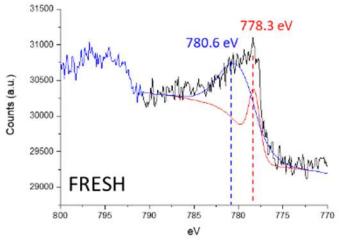

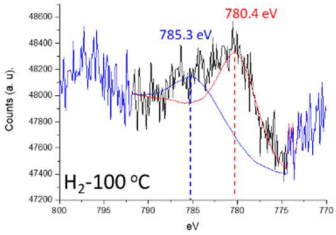

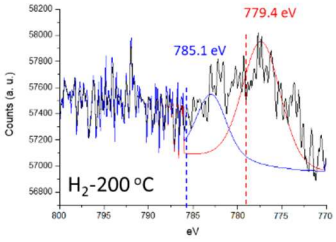

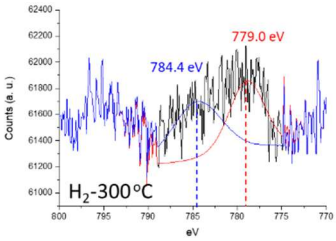

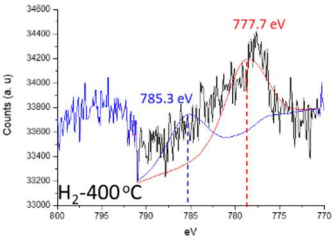

Fe species

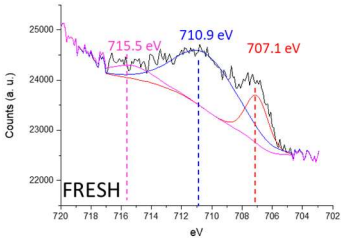

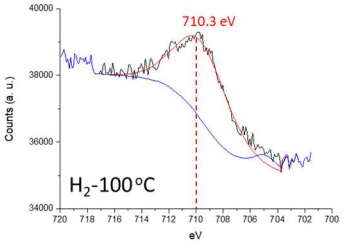

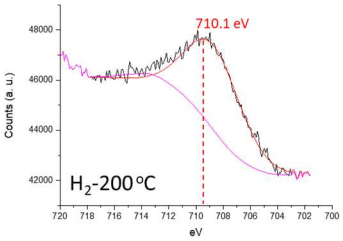

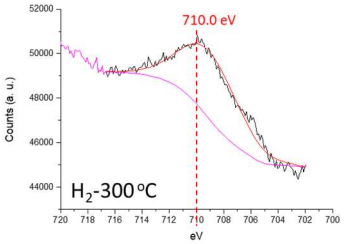

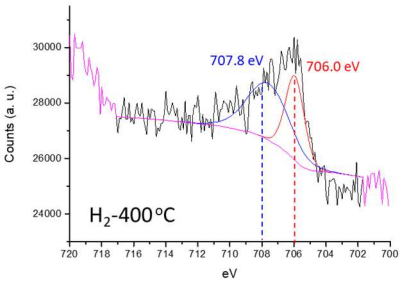

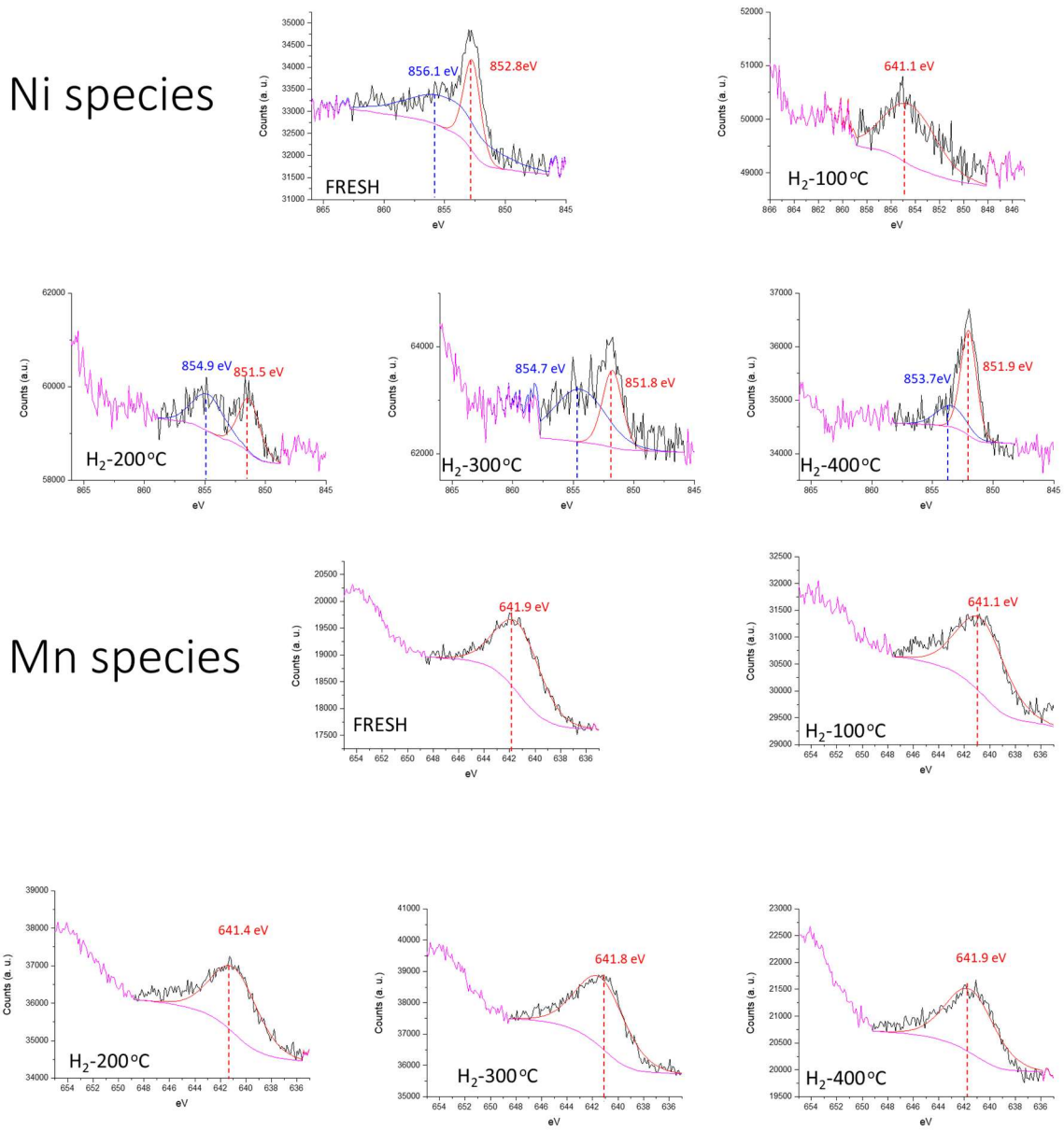

Fig. S14 X-ray photoelectron spectroscopy (XPS) data analysis of each metal from HMEA-700 sample fresh, after exposition to H_2 at 100, 200, 300 and 400 ^{0}C.

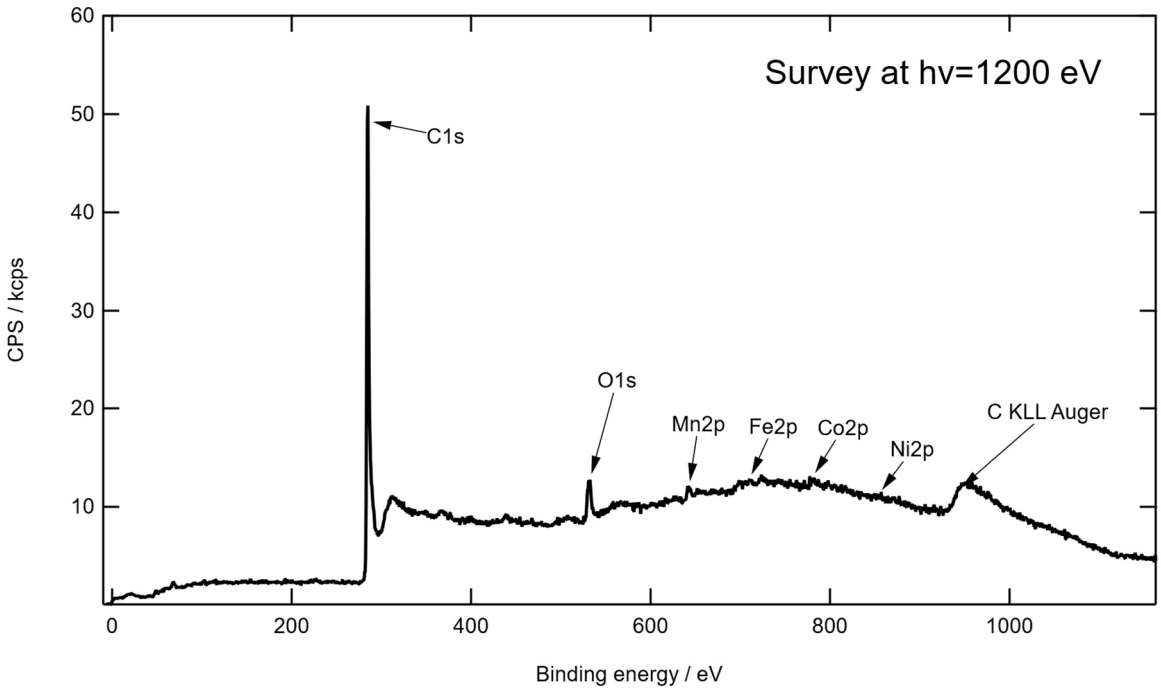

Fig. S15 X-ray photoelectron spectroscopy (XPS) survey scan at hυ=1200 eV and pass energy of 80 eV of the as-loaded HMEA-800 powder drop cast on Au foil.

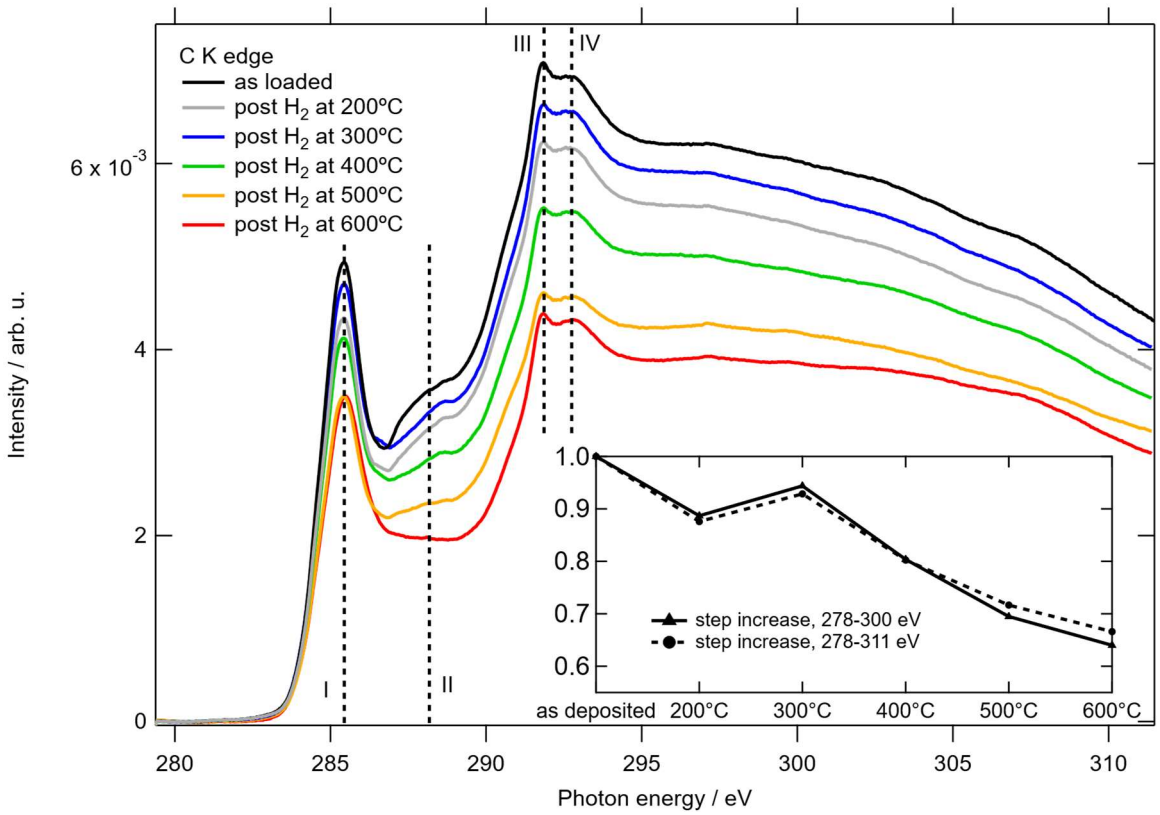

Fig. S16 Near edge X-ray absorption fine structure (NEXAFS) spectra of the C K edge from HMEA powder as-loaded and after increasingly higher annealing in H_2. A pre-edge constant background has been subtracted. The inset shows the C K edge step increase as a function of temperature (normalised to the edge jump of the as-loaded sample); a clear decrease as a function of annealing temperature is seen.

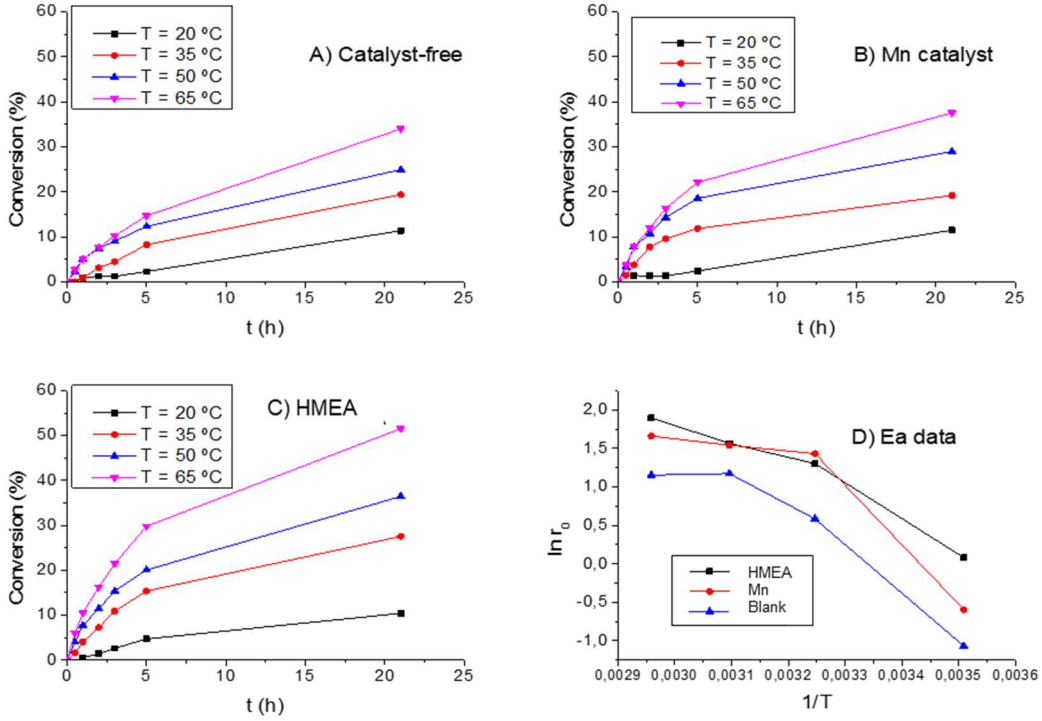

Fig. S17 Oxidative cleavage of styrene performed at different temperatures. Conditions: 1 mmol of styrene **2a**. 1.1 eq. *t*-BuOOH. hexane (1M). (a) Catalyst-free; (b) Mn catalyst (10 mg. 0.65 mol% Mn); (c) HMEA-700 (2.5 mg. 0.65 mol% Mn); (d) Arrhenius curves for the activation energy (E_a) calculation.

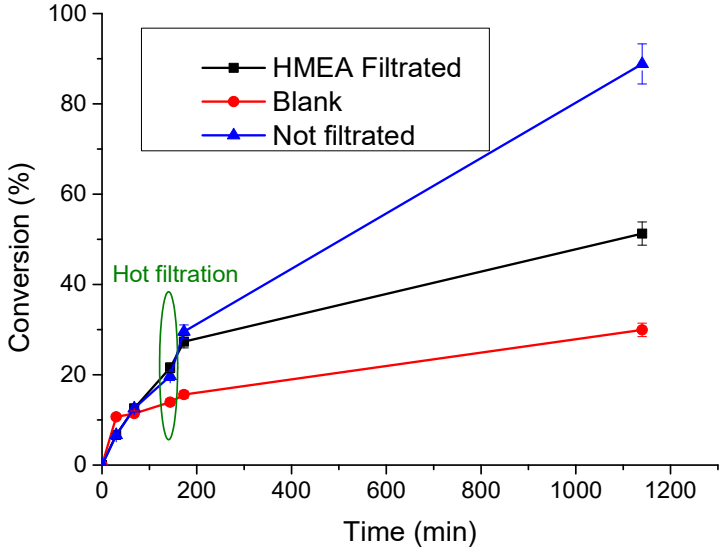

Fig. S18 Hot filtration test for the oxidative cleavage of styrene **2a** catalysed by HMEA-700. The activity of the leached species is calculated with the slope difference between the hot filtration test, the blank test and the test with the solid catalyst. Error bars account for a 5% uncertainty.

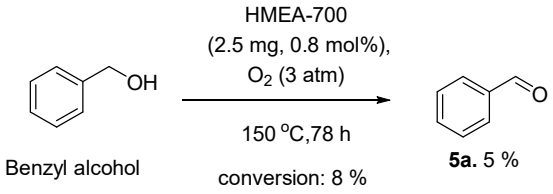

Fig. S19. Result for the aerobic oxidative dehydrogenation reaction of benzyl alcohol in the presence of the HMEA-700 catalyst.

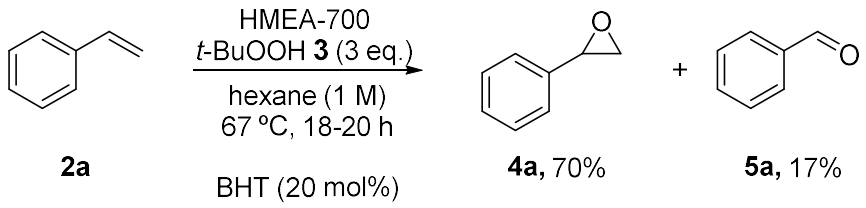

Fig. S20 Oxidative cleavage catalysed by HMEA-700 with 3 equivalents of *t*-BuOOH using 2,6-di-*tert*-butyl-4-methylphenol (BHT) as radical scavenger. Yield (**4a**,**5a**) calculated by GC, using *n*–dodecane as internal standard. Conditions: 1 mmol styrene **2a**, 3 equiv. of *t*–BuOOH **3**, 0.2 mmol BHT, 1 mL hexane.

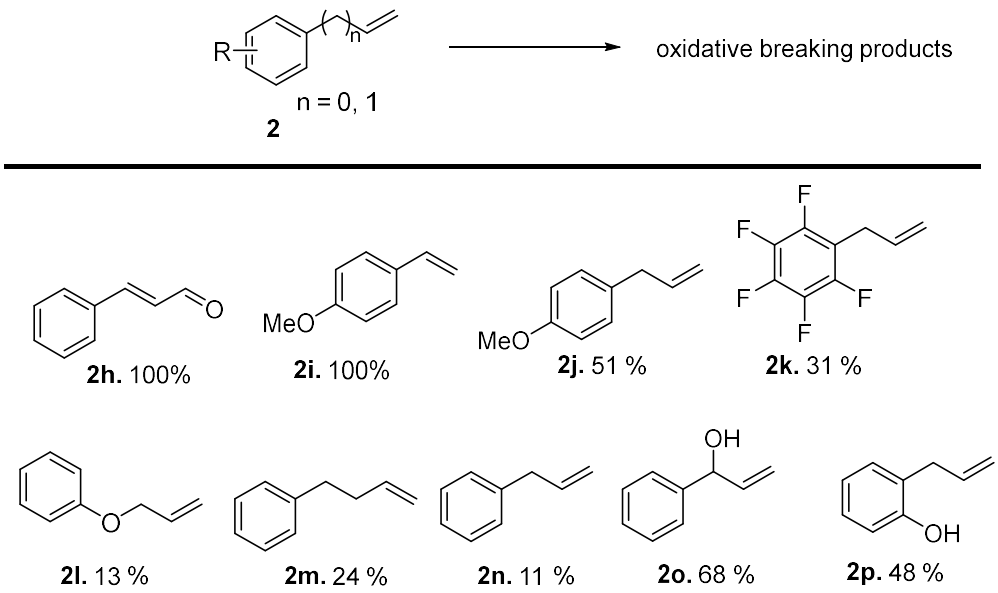

Fig. S21 Scope of the HMEA-700 catalysed oxidative cleavage of alkenes. Yields calculated by GC, using *n*-dodecane as internal standard. Conditions: 1 mmol alkene **2**, 3 eq of *t*-BuOOH **3**, 1 mL hexane, 2.5 mg HMEA-700 (0.65 mol%), 67 ºC, 18-20 h.

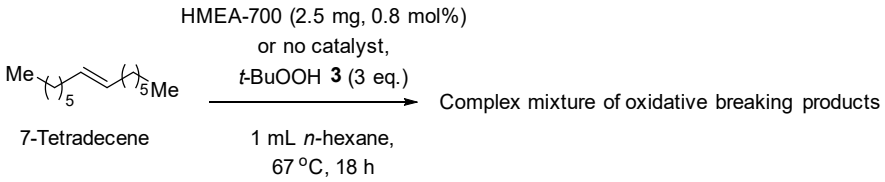

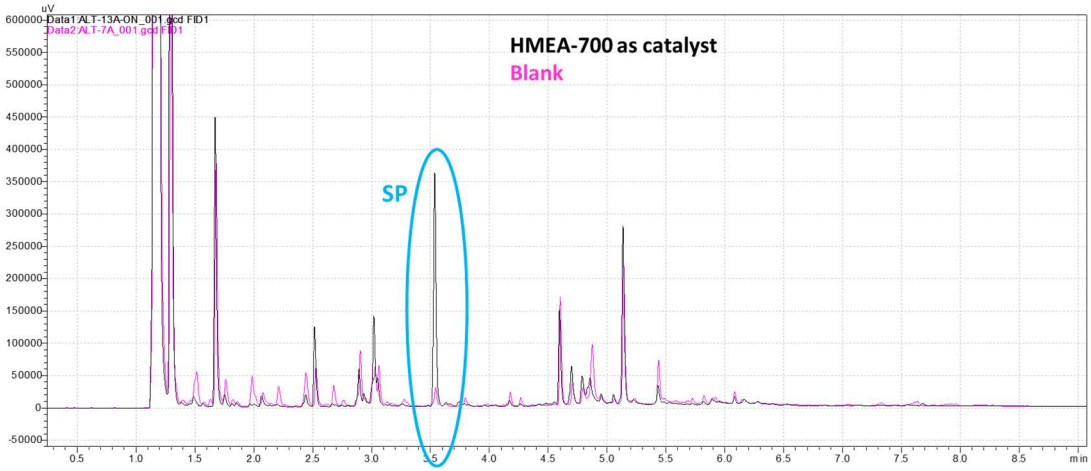

Fig. S22. Results for the oxidation of 7-tetradecene in the presence or not of the HMEA-700 catalyst.

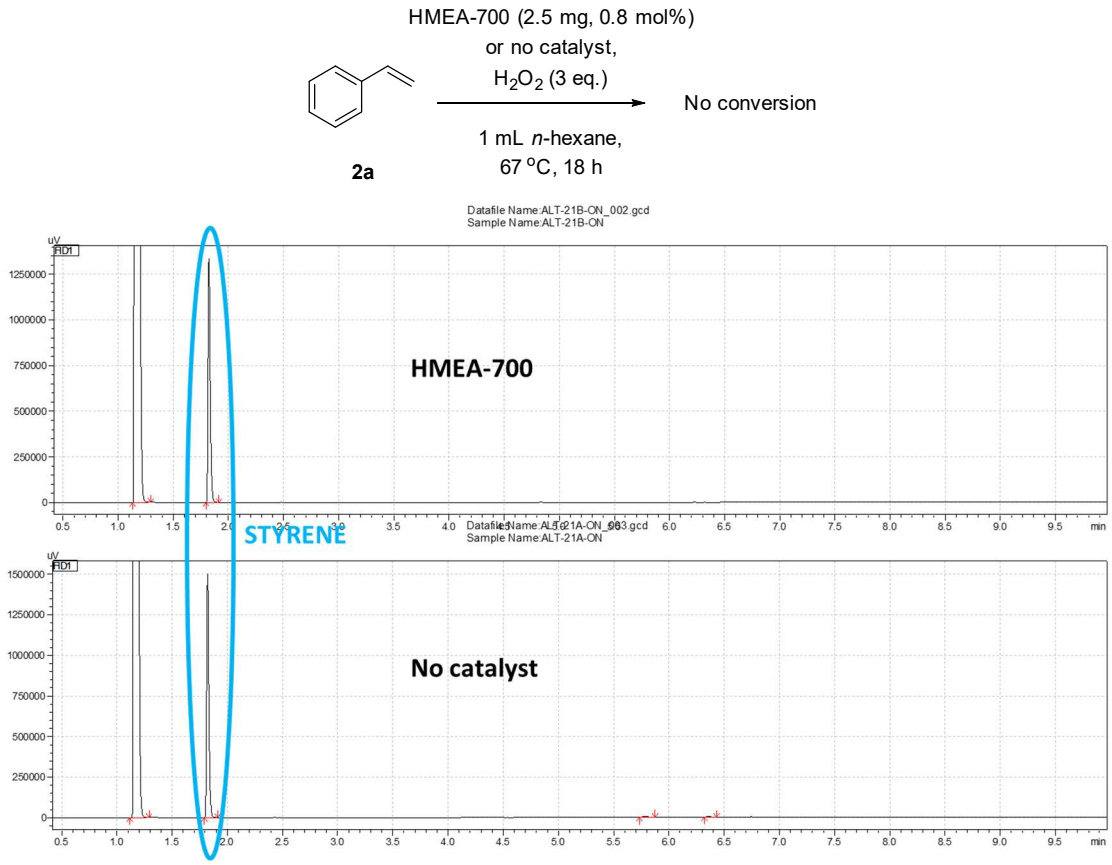

Fig. S23. Attempt of oxidation with H_2O_2 in the presence or not of the HMEA-700 catalyst.

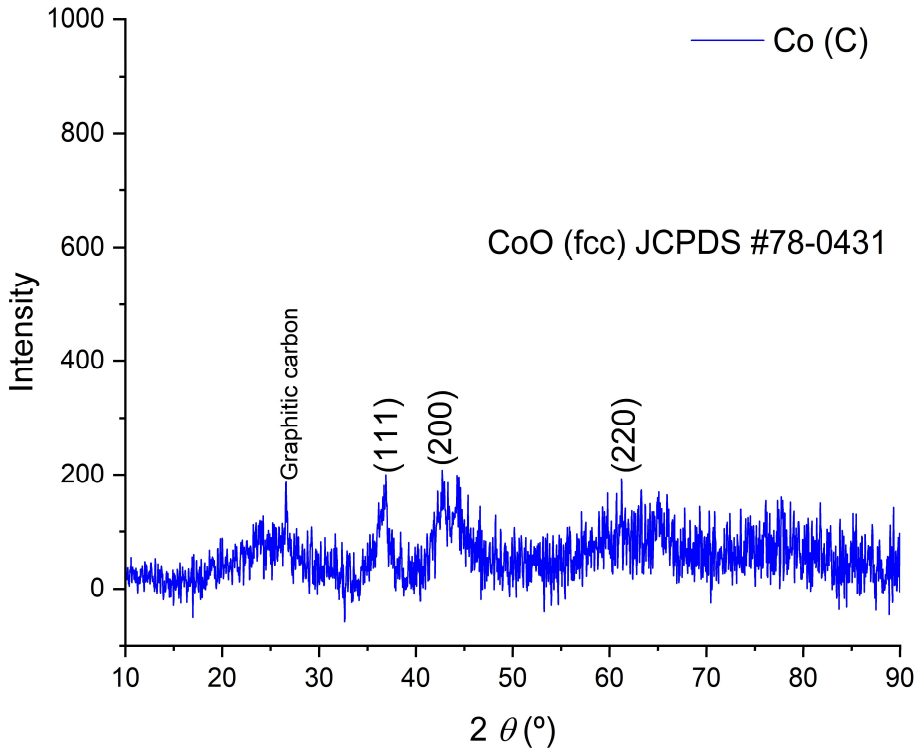

Fig. S24 Carbon–supported Co NPs (**Co (C)**) characterization by powder X-ray diffraction (PXRD). Co(II) oxide phase observed. Inductively coupled plasma optical emission spectroscopy (ICP-OES) analysis indicates a concentration in Co of 11.70 wt%.

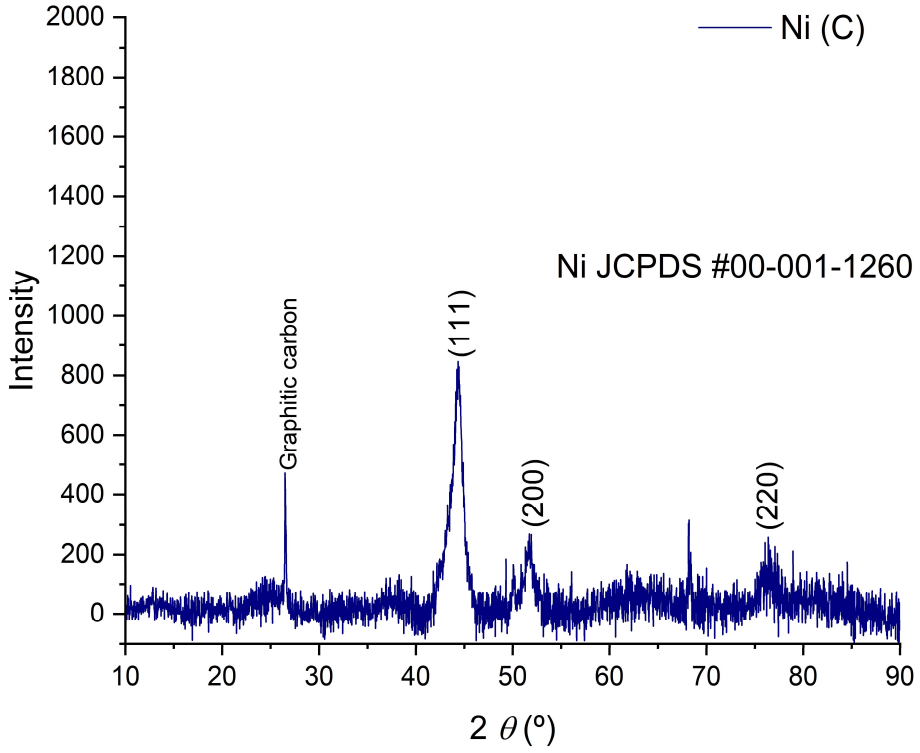

Fig. S25 Carbon–supported Ni NPs (**Ni (C)**) characterization by powder X-ray diffraction (PXRD). Ni(0) phase observed. Inductively coupled plasma optical emission spectroscopy (ICP-OES) analysis indicates a concentration in Ni of 11.90 wt%.

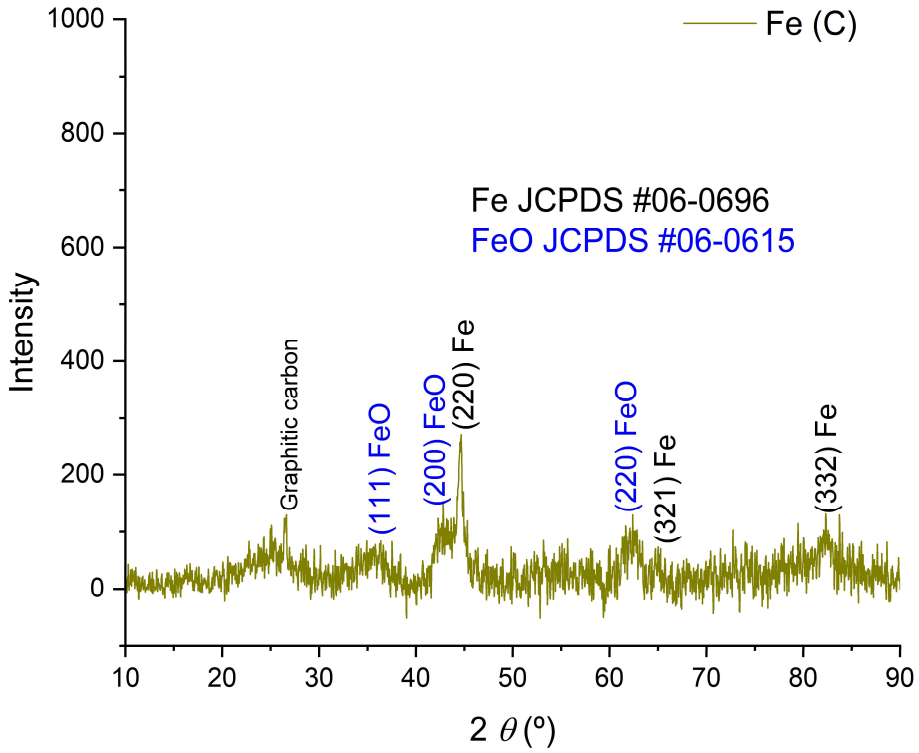

Fig. S26 Carbon–supported Fe NPs (**Fe (C)**) characterization by powder X-ray diffraction (PXRD). Fe(0) and Fe(II) oxide phases observed. Inductively coupled plasma optical emission spectroscopy (ICP-OES) analysis indicates a concentration in Fe of 10.25 wt%.

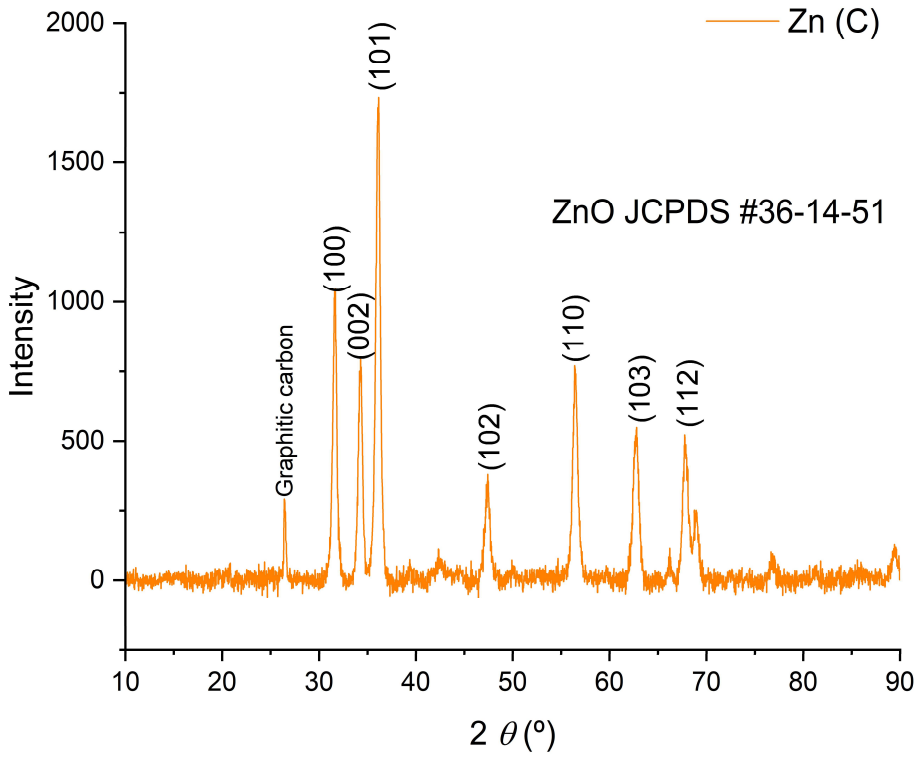

Fig. S27 Carbon–supported Zn NPs (**Zn (C)**) characterization by powder X-ray diffraction (PXRD). ZnO phase observed. Inductively coupled plasma optical emission spectroscopy (ICP-OES) analysis indicates a concentration in Zn of 11.19 wt%.

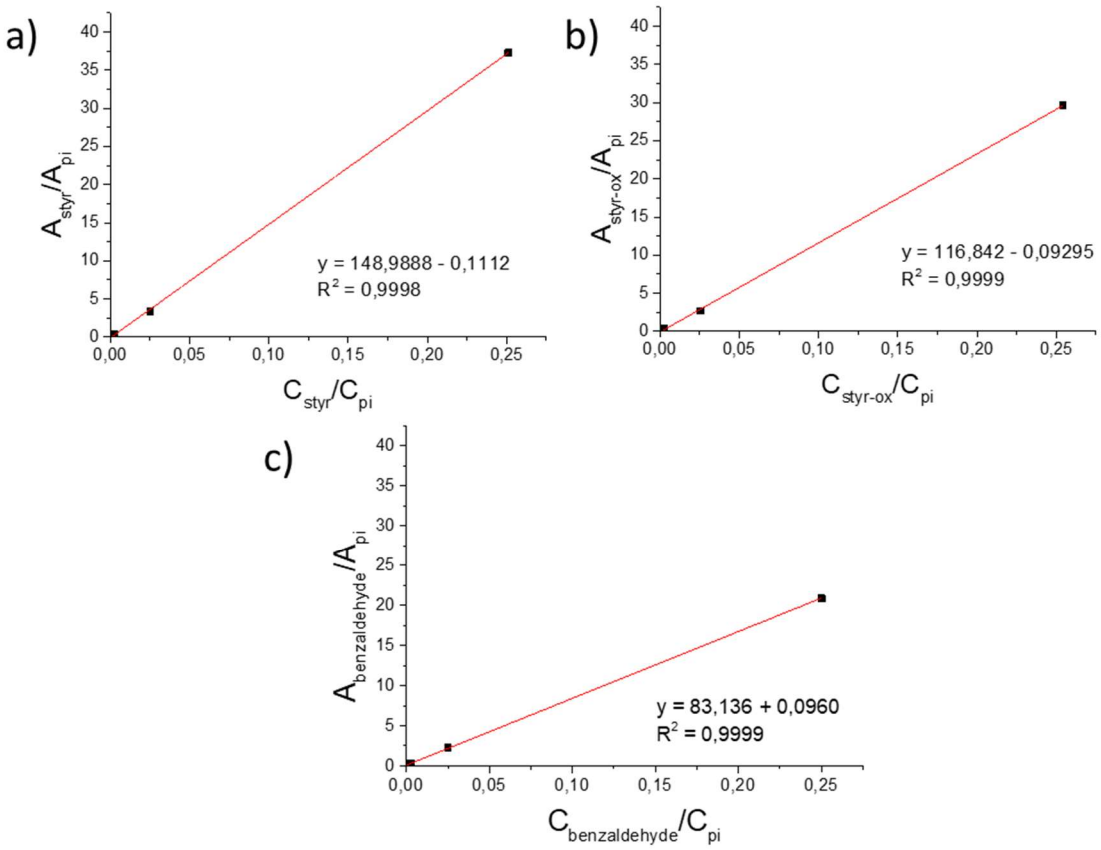

Fig. S28 Calibration curves for: a) styrene **2a**, b) styrene oxide **4a**, c) benzaldehyde **5a**. The response factors are 1.0000, 0.7842 and 0.5580 respectively, normalizing respect to styrene **2a**.

3. Supplemental References

S1. C. Annese, D. Caputo, L. D'Accolti, C. Fusco, A. Nacci, A. Rossin, G. Tuci and G. Giambastiani, *Eur. J. Inorg. Chem.,* **2019**, *2*, 221–229.

S2. J.–Q. Yu and E. J. Corey. *Org. Lett.,* **2002**, *4*, 2727–2730.

S3. M. Fadhli, I. Khedher and J. M. Fraile, *C. R. Chimie,* **2017**, *20*, 827–832.

S4. K. Jasiak, T. Krawczyk, M. Pawlyta, A. Jakóbik-Kolon and S. Baj, *Catal. Lett.* **2016**, *146*, 893-901.

S5. S. S. Pawar, R. N. Ketkar, P. B. Gaware, K. U. Jagushte, D. Dhawne, S. N. Save, S. Sharma, G. Periyasamy, N. Chimthanawala, S. Sathaye, S. V. Joshi and N. Sadhukhan, *Dalton Trans.* **2024**, *53*, 5770-5774.

S6. H. Koizumi, M. Tanabe, T. Kambe, T. Imaoka, W.-J. Chun and K. Yamamoto, *Chem. Lett.* **2022**, *51*, 317-320.

S7. X. Gao, J. Lin, L. Zhang, X. Lou, G. Guo, N. Peng, H. Xu and Y. Liu, *J. Org. Chem.* **2021**, *86*, 15469-15480.

S8. G. Hu, W. Chang, S. An, B. Qi and Y.-F. Song, *Chin. Chem. Lett.* **2022**, *33*, 3968-3972.